Title

Intraoperative delineation of p16+ oropharyngeal carcinoma of unknown primary origin with fluorescence lifetime imaging: Preliminary report

Journal

Head & Neck, 44(8)

ISSN

1043-3074

Authors

Weyers, Brent W

Birkeland, Andrew C

Marsden, Mark A

et al.

Publication Date

2022-08-01

DOI

10.1002/hed.27078

Peer reviewed

Received: 9 November 2021 | Revised: 23 February 2022 | Accepted: 22 April 2022

DOI: 10.1002/hed.27078

WILEY

ORIGINAL ARTICLE

Intraoperative delineation of p16+ oropharyngeal carcinoma of unknown primary origin with fluorescence lifetime imaging: Preliminary report

Brent W. Weyers BS[1] | **Andrew C. Birkeland MD**[2] | **Mark A. Marsden PhD**[1] | **Athena Tam BS**[1] | **Julien Bec PhD**[1] | **Roberto P. Frusciante BA**[1] | **Dorina Gui MD, PhD**[3] | **Arnaud F. Bewley MD**[2] | **Marianne Abouyared MD**[2] | **Laura Marcu PhD**[1] | **Donald Gregory Farwell MD**[2,4]

[1]Department of Biomedical Engineering, University of California, Davis, Davis, California, USA

[2]Department of Otolaryngology – Head & Neck Surgery, University of California, Davis, Davis, California, USA

[3]Department of Pathology and Laboratory Medicine, University of California, Davis, Davis, California, USA

[4]Department of Otorhinolaryngology – Head and Neck Surgery, University of Pennsylvania, Philadelphia, Pennsylvania, USA

Correspondence
Donald Gregory Farwell, Department of Otorhinolaryngology – Head and Neck Surgery, Perelman School of Medicine, University of Pennsylvania, 3400 Spruce St, Ravdin 5, Philadelphia, PA 19104, USA.
Email: greg.farwell@pennmedicine.upenn.edu

Laura Marcu, Department of Biomedical Engineering, University of California, Davis, 451 Health Sciences Drive, GBSF 2303, Davis CA 95616, USA.
Email: lmarcu@ucdavis.edu

Funding information
National Institutes of Health, Grant/Award Number: R01 CA187427

Abstract

Background: This study evaluated whether fluorescence lifetime imaging (FLIm), coupled with standard diagnostic workups, could enhance primary lesion detection in patients with p16+ head and neck squamous cell carcinoma of the unknown primary (HNSCCUP).

Methods: FLIm was integrated into transoral robotic surgery to acquire optical data on six HNSCCUP patients' oropharyngeal tissues. An additional 55-patient FLIm dataset, comprising conventional primary tumors, trained a machine learning classifier; the output predicted the presence and location of HNSCCUP for the six patients. Validation was performed using histopathology.

Results: Among the six HNSCCUP patients, p16+ occult primary was surgically identified in three patients, whereas three patients ultimately had no identifiable primary site in the oropharynx. FLIm correctly detected HNSCCUP in all three patients (ROC-AUC: 0.90 ± 0.06), and correctly predicted benign oropharyngeal tissue for the remaining three patients. The mean sensitivity was $95\% \pm 3.5\%$, and specificity $89\% \pm 12.7\%$.

Conclusions: FLIm may be a useful diagnostic adjunct for detecting HNSCCUP.

KEYWORDS

cancer delineation, endogenous autofluorescence, fluorescence lifetime imaging (FLIm), intraoperative surgical guidance, machine learning in oncology applications, occult primary tumor, oropharyngeal cancer of unknown primary origin, p16+ squamous cell carcinoma, transoral robotic surgery

1 | INTRODUCTION

Head and neck squamous cell carcinoma of unknown primary origin (HNSCCUP), also known as occult primary, is defined as the occurrence of squamous cell carcinoma in cervical lymph nodes with no primary site identified.[1] These cases (~2600 annually in the United States) represent approximately 3%–5% of all new cases of head and

neck squamous cell carcinoma, and are considered unknown after exhaustive clinical, radiographic, and surgical evaluation.[2–6] HNSCCUP is disproportionately correlated to positive human papillomavirus (HPV) status and exhibits weaker association to tobacco and alcohol abuse.[7,8] Statistically, most HPV+ HNSCCUP patients are male, white, nonsmokers, and nondrinkers.[4,9] HPV-mediated tumors aberrantly overexpress p16 biomarkers; thus, p16 immunohistochemistry is recommended for determining HNSCCUP etiology.[10]

It is critically important to locate the primary site in these patients to reduce treatment-related morbidity via more anatomically focused interventions.[7,11] Most HNSCCUP cancers are eventually located in the cryptic lymphoepithelium of the palatine tonsils and the lingual tonsils of the base of tongue.[4,5,8] Traditional surgical assessments of these cases included bilateral tonsillectomy and base of tongue biopsies in efforts to locate the primary tumor.[8,12] Recent publications in the HPV era have suggested the appropriateness of only performing an ipsilateral tonsillectomy in the workup of these patients.[13] The adoption of transoral robotic surgical platforms (TORS) in the workup of HNSCCUP has facilitated improved HNSCCUP detection rates[4,14–16]; however, depending on the diagnostic and clinical capabilities of different medical institutions, more than 50% of primary tumors may remain undiscovered for patients with HNSCCUP.[12] To improve intraoperative decision-making and enhance the detection of these elusive tumors, new diagnostic technologies compatible with TORS are needed.

Fluorescence lifetime imaging (FLIm) is an emerging label-free imaging technique for real-time tissue diagnosis. Recently, FLIm has been integrated into both the da Vinci Si[17,18] and SP.[18,19] TORS platforms have demonstrated promise for the intraoperative delineation of conventional primary oral cavity and oropharyngeal cancers in human patients, both in vivo and ex vivo.[17,19,20] FLIm has also demonstrated potential for disease diagnosis and surgical guidance in other surgical areas, including cardiovascular disease,[21–23] breast cancer,[24] brain cancer,[25] and intraoperative guidance during thyroid surgery.[26] While FLIm technology is still in investigational stages from a clinical standpoint, significant developments in optical hardware, classification methods, and computing power are rapidly facilitating FLIm towards clinical adoption.[27]

FLIm relies on the strong fluorescence emission from endogenous fluorophores (e.g., collagen crosslinks in the stroma and metabolic cofactors nicotinamide adenine dinucleotide (NADH) and flavin adenine dinucleotide (FAD) in cells) upon ultraviolet light excitation.[28] FLIm instrumentation can evaluate both time-resolved fluorescence characteristics and spectral intensities. Time-resolved characteristics are assessed by computing the fluorescence lifetime, which measures the time which tissue fluorophores spend in the excited quantum state after laser excitation before returning to the ground state by emitting a photon. Typically, the lifetime of endogenous fluorophores ranges from sub-nanoseconds to 5–7 nanoseconds. Collectively, endogenous fluorophores exhibit fluorescence lifetime sensitivity to numerous chemical and physical factors such as pH, oxygenation, temperature, solvent polarity, and binding to macromolecules.[29] By taking advantage of alterations in tissue structural and metabolic characteristics associated with neoplastic processes,[28,30] FLIm has the ability to provide holistic information about tissue molecular composition to facilitate the detection of neoplastic tissue.

While FLIm has not been specifically developed as a tool for identifying unknown primary tumors, the recent success of this technology for demarcating conventional primary oropharyngeal tumors[19,20,27] has motivated the present investigation of discriminatory performance in HNSCCUP patients. Specifically, we investigated whether the addition of FLIm to standard diagnostic workups could enhance the detection of primary lesions within p16+ HNSCCUP patients. To our knowledge, this is one of the earliest studies to integrate a supplemental imaging approach with TORS to enhance occult primary tumor detection. One other group has made notable progress in this area using narrowband imaging (NBI) on an 8-patient HNSCCUP cohort.[31]

This study aimed to conduct intraoperative FLIm measurements on patients with TORS-facilitated extirpation of HNSCCUP to identify the presence of occult primary tumors not identified by standard-of-care workup. FLIm was integrated into the da Vinci SP and deployed for acquiring measurements on oropharyngeal tissues with a high propensity for harboring the primary tumor (i.e., palatine and lingual tonsils).[4,5,8] We sought to test the hypothesis that intraoperatively acquired FLIm measurements output from a machine learning classifier can successfully detect p16+ occult primaries presenting in the mucosa (<250 μm from tissue surface) and differentiate such malignancies from healthy tissue.

2 | METHODS

This study comprises an $N = 61$ patient dataset evaluating FLIm for diagnosis and surgical guidance of oral cavity and oropharyngeal cancers. Of the 61-patients, 55 comprised conventional primary tumors of the oropharynx, whereas the other 6 patients were classified with p16+ HNSCCUP after exhaustive diagnostic workup. Procedures were approved by the University of California, Davis

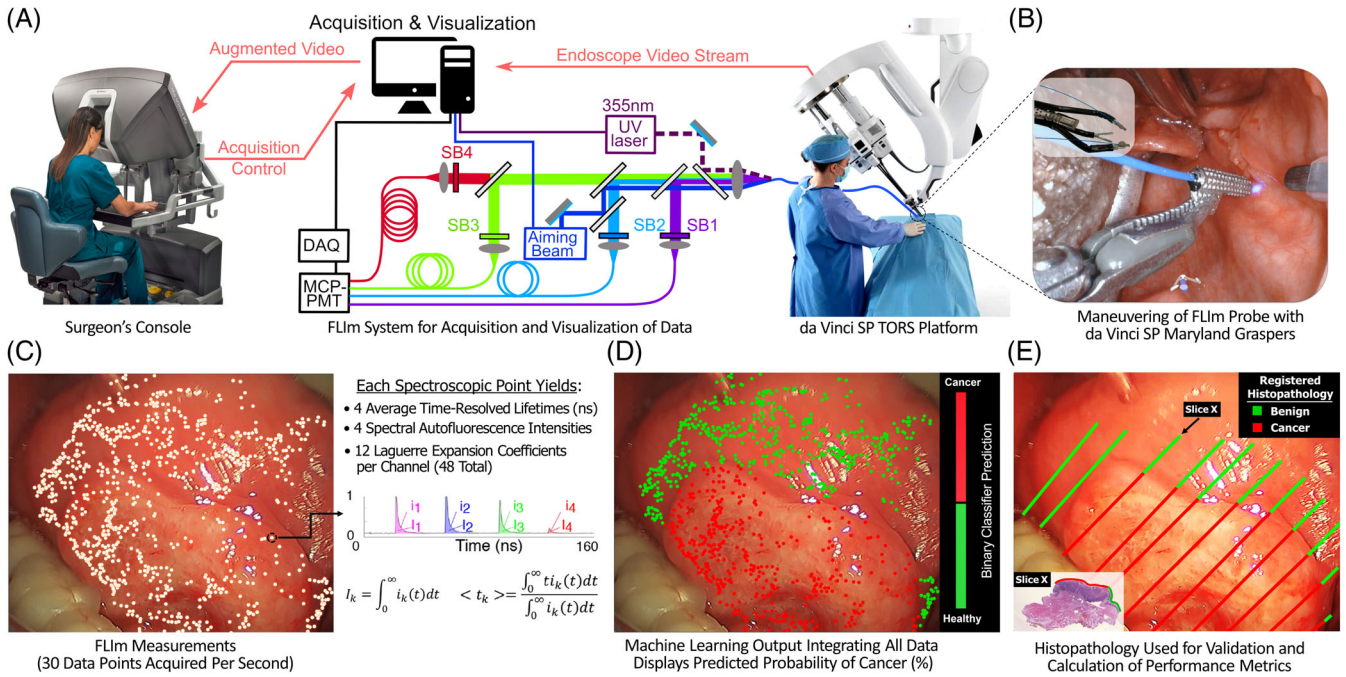

FIGURE 1 Overview of FLIm instrumentation, data aquisition, classification, and validation to histopathology. (A) Schematic of FLIm instrumentation and integration into the da Vinci SP TORS platform. The instrument features a 355 nm excitation laser delivering light through a multimode fiber optic cable to tissues within a surgical region of interest. Resulting autofluorescence is transmitted back to a wavelength selection module, comprising four channels which capitalize on the peak autofluorescence of collagen, NADH, FAD, and porphyrins. (B) Illustration of the integration of the fiber optic probe into the da Vinci SP surgical robot, held by Maryland Bipolar Forceps. The operator at the surgical console manipulates the fiber optic probe with the robotic instruments to conduct a scan of approximately 1 min over a surgical region of interest. An aiming beam is used to create blue visible laser light on the tissue to localize where point-spectroscopic measurements are acquired. (C) Illustration of augmented FLIm data points over a patient's tongue tissue, selected from one of the $N = 55$ patients used to train the classifier. As illustrated in the subfigure, each data point yields 56 possible analytical metrics. The corresponding example waveforms and calculations for spectral intensity I_K and lifetime $<t_K>$ are demonstrated on the right. (D) Machine learning output from integrating all data at each spectroscopic point-measurement to predict cancer probability. (E) Histopathology from the excised specimen registered in vivo to validate and quantify performance metrics (ROC-AUC, sensitivity, and specificity) of the FLIm device. [Color figure can be viewed at wileyonlinelibrary.com]

Institutional Review Board (IRB ID#800853) and conducted in accordance with the Code of Ethics of the World Medical Association for experiments involving humans.

2.1 | Study design and inclusion/exclusion criteria of patients

Eligible patients presenting to UC Davis Otolaryngology – Head & Neck Surgery department were recruited in the study over a 2-year period from May 2019 to April 2021 without demographic or prognostic consideration. Patients with a preoperative diagnosis of HNSCCUP were eligible for this study. Patients were classified as presenting with HNSCCUP after an exhaustive clinical, radiographic, and surgical evaluation did not identify the primary tumor site; this includes negative PET and CT findings, absence of tactile cues when palpating tissue, lack of visual identification by endoscopy, and negative directed biopsies at suspicious areas.

Exclusion criteria consisted of (1) pediatric patients based on IRB considerations, (2) patients with positive HIV status from a safety standpoint for research personnel, (3) individuals with previous major head & neck surgery where extensive scarring may be present, and (4) patients with known use of orally administered crack-cocaine or methamphetamine (MA), which imparts severe adverse effects on oral tissues and confounds FLIm measurements.[32] HNSCCUP patients with p16− cancer were not assessed within the scope of this manuscript (as HPV-negative disease represents a different entity).

One prospective p16+ HNSCCUP patient resided within the study's exclusion criteria, and therefore was not analyzed (see discussion) due to their known recurring use of orally administered methamphetamine (MA). In total, $N = 6$ p16+ HNSCCUP patients met the

inclusion criteria for the study and provided their informed consent to participate in this research.

2.2 | FLIm instrumentation

Figure 1A illustrates the custom-built, fiber-based, point-scanning FLIm system with corresponding integration into the da Vinci SP surgical system. In-depth characterizations of this instrument and specifications are detailed extensively elsewhere.[17,19,33–35] Briefly, the FLIm system features a 365-μm core multimode optical fiber which delivers 355 nm pulsed UV laser excitation light at a 120-Hz repetition rate to biological tissue. The optical fiber's distal end features a 3D printed stainless steel grasper, which is held and maneuvered by the da Vinci SP robotic system's instruments (Figure 1B). The same optical fiber is used to relay autofluorescence point-measurements from the tissue regions evaluated to the FLIm system. The fiber's proximal collection end is coupled to a wavelength selection module (WSM) which features a set of four dichroic mirrors and bandpass filters (i.e., CH1: 390 ± 20 nm, CH2: 470 ± 14 nm, CH3: 542 ± 25 nm, and CH4: 629 ± 26.5 nm) used to spectrally resolve the autofluorescence signal.[34,35] These spectral bands capitalize on the autofluorescence emission maxima the endogenous fluorophores collagen, NAD(P)H, FAD, and porphyrins, which are reported as the main contributors to H&N cancer autofluorescence emission.[19,20,28] The optical signal from each spectral band was time-multiplexed onto a single microchannel plate photomultiplier tube, amplified, and time-resolved by a high sampling frequency digitizer at 80 ps intervals. A separate visible 445 nm laser, integrated into the WSM, highlights the location where FLIm point measurements are acquired. This enables the overlay of optical data points on white light images. This pulse sampling FLIm approach is suitable for use in the presence of external illumination such as operating room lights.[34,35]

Because this is a point-scanning technology, the field-of-view can be as large as the entire visualized surgical area (multiple centimeter scale) from the da Vinci SP. When scanning directly adjacent to tissue, the spatial resolution of the device is determined by the fiber core size (365 μm) and the probe-to-tissue distance, yielding a resolution between 0.6 ± 0.2 mm depending on the distance of the probe to the tissue surface. The peritumoral region has many morphologic and phenotypic distinctions from non-tumor-bearing healthy tissue, including altered pH levels, metabolic characteristics, and oxygenation gradients, extending up to 1 cm from the margins of tumor tissue.[36] Correspondingly, although the penetration depth of the UV laser is approximately 250 μm, the secondary tissue effects from neoplasms extend multiple millimeters beyond the cancer site, potentially allowing FLIm to detect cancers beyond the absolute penetration depth of the UV laser; this has yet to be formally evaluated.

2.3 | Data collection

FLIm scanning was conducted after patients were anesthetized, intubated, and prepared for TORS. Intraoperative biopsies were conducted after FLIm scanning to mitigate any potential confounding effect on the data. The da Vinci SP was introduced into the patient's oral cavity and the sterile optical fiber's distal end was grasped and actuated by the robot's Maryland graspers (Figure 1B). In vivo scans of approximately 90 s in duration were conducted bilaterally over palatine tonsils and the base of tongue regions to generate spectroscopic data overlaid over white light images. An example of this spectroscopic data overlay on a patient's tongue tissue (used in the classifier training dataset) is illustrated in Figure 1C. The fiber optic probe was then removed from the patient, and the surgeon proceeded with en bloc excision of tissues suspected of occult primary. This typically included a bilateral tonsillectomy followed by biopsies and/or lingual tonsillectomy depending on the surgeon's discretion. Excised specimens were sectioned in a pathology grossing room to generate multiple sequential H&E slides for pathologic interpretation; these slides included a combination of both frozen and permanent sections. HPV status was assessed by using p16 immunohistochemistry.

2.4 | Calculations and analysis of data

Average lifetime estimation for each spectral band was performed using constrained least square deconvolution with Laguerre expansion. This fast and robust technique has been detailed extensively.[33] Briefly, the pulsed UV laser repetition rate of 120 Hz determines the FLIm measurement speed. The FLIm waveforms which originate from each spectral measurement are averaged four times before further processing, leading to 30 averaged spectroscopic data points acquired each second. For each of the four spectral bands of the instrument, the average lifetime value, spectral intensity, and 12 fitting coefficients of the Laguerre expansion are computed (Figure 1C). Spectral properties of the fluorescence emission are also estimated by computing the relative intensity of each spectral channel of the instrument. This leads to a total of 56 parameters (4 time-resolved average lifetimes, 4 spectral intensity ratios, and 48 expansion metrics).

A random forest machine learning classifier estimated the probability of healthy versus cancer for each point-

measurement.[37] This classifier was trained on the larger 55-patient cohort of known primary oropharyngeal tumors (38 palatine tonsil and 17 base of tongue patients) and then applied to make predictions on the measurements obtained from HNSCCUP patients. Sensitivity and specificity were calculated by standard convention. ROC-AUC quantified the true positive rate versus false positive rate of individual spectroscopic point-measurements based on histological findings. This approach builds up on the development of predictors previously described elsewhere (Figure 1D).[20] The unit of analysis for statistical evaluation consists of binary predictors (i.e., cancer vs. healthy) output from machine learning classification for individual spectroscopic data points acquired over a surgical region of interest. This type of analysis is distinct from region/lesion-based assessment, where multiple measurements are combined to predict the nature of a preidentified region. This approach typically leads to better sensitivity and specificity numbers, however, requires a priori knowledge of the extent of the lesions.

2.5 | Coregistration and histopathological validation of data

Registration of data to histopathology is detailed in our prior work.[19] In brief, a pathologist (DG) digitally annotated H&E slides using *Aperio (Leica) Imagescope* viewing software. Features within 250 μm of the tissue's mucosal surface were annotated, corresponding approximately to the maximum penetration depth of the laser. The following annotation labels were used: (1) carcinoma, (2) lymphoid tissue, and (3) benign tissue. Label 1 was treated as the positive class (i.e., cancer) and labels 2 and 3 were treated as the negative class (i.e., benign) from an analysis standpoint. Histopathology sections were overlaid onto a high-resolution image of the excised specimen, accounting for compression and expansion registration artifacts between histology and the excised specimen. An in vivo recording of the surgical excision process was used to facilitate registration of the excised specimen to the original in vivo environment. This histopathological data was then overlaid onto a reference image in vivo (Figure 1E). To account for motion between the TORS surgical camera and the evaluated tissue, a novel motion compensation algorithm was applied.[18] Quantification of performance was based only on regions with coregistered histopathology.

3 | RESULTS

Table 1 depicts all patient demographics, pertinent clinical characteristics, and surgical outcomes of the enrolled patient population. An average of 2355 FLIm spectroscopic data points (ranging between 1393 and 4793) were acquired from each of the six patients. Three patients (Patients 1–3) presented with HNSCCUP (all p16+) within the regions where FLIm scans were performed. Patient 6 did have p16+ HNSCCUP near the FLIm scan area, however the region of cancer was outside the area of the research scan, thus only FLIm data for benign tissue was acquired. All other patients enrolled in the study presented with HNSCCUP, however no oropharyngeal primary was identified with TORS. Each patient had multiple tissues excised where some of these tissues contained the occult primary and others were benign, as presented in Table 1. Patients 4–6 only had benign tissue imaged in the FLIm scan area, thus only specificity is calculated for these patients due to the absence of the positive data class (i.e., cancer). Only tissue areas validated with histopathology were used to calculate ROC-AUC, sensitivity, and specificity.

Table 2 presents ROC-AUC, sensitivity, and specificity calculations for each patient. FLIm correctly detected the presence of the occult primary in all three patients (Patients 1–3), yielding a mean ROC-AUC score of 0.90 ± 0.06. The extent of the cancer (quantified by sensitivity) was detected with a mean of 95% ± 3.5%. The method however demonstrated mixed specificity results for these patients. Patients 4–6 comprised data from benign tissues only, where the FLIm classifier correctly demarcated the entire extent of all tissues as benign and output a mean specificity of 99% ± 1%. All six patients together, which includes the three patients with p16+ SCC within the FLIm scan area and the three patients with only benign tissue evaluated, resulted in a classification specificity of 89% ± 12.7%.

Figure 2 presents case studies for all three patients with p16+ HNSCCUP imaged by FLIm. Each patient case study displays both the binary probability of cancer for each acquired spectral point-measurement and the patient's corresponding registered histopathology in vivo. Figure 3 presents case studies for all three patients who did not have cancer imaged within the FLIm scan area (i.e., only benign tissue evaluated). Like Figure 2, this figure displays the binary probability of cancer classifier output and the patient's corresponding registered histopathology in vivo. A specific media example (Video S1, Supporting Information) is provided to demonstrate the real-time cancer classification output for Patient 4 (featured in Figure 3A), where the FLIm classifier correctly demarcates tissue uninvolved with HNSCCUP.

4 | DISCUSSION

Collectively, the results demonstrate FLIm's clinical value in the surgical management of p16+ HNSCCUP in

TABLE 1 Demographics, clinical characteristics, and surgical outcomes of the study population

		Patient 1	Patient 2	Patient 3	Patient 4	Patient 5	Patient 6
Demographics	Gender	Male	Male	Male	Male	Male	Male
	Age at surgery	63	74	59	62	77	69
	Race	White	White	White	White	White	White
	Ethnicity	Not Hispanic	Not Hispanic	Not Hispanic	Not Hispanic	Not Hispanic	Not Hispanic
Pertinent clinical characteristics	Alcohol use	2 DPD	3 DPD	Infrequent	Infrequent	1 DPD	3 DPD
	Tobacco use	Never smoker	0.25 PPD (quit 2011)	Never smoker	Never smoker	0.5 PPD (current)	0.5 PPD (quit 2014)
	Illicit drug use	No	No	No	No	No	Cannabis (daily)
Surgical outcomes	Postoperative occult primary diagnosis	p16+ SCC	p16+ SCC	p16+ SCC	p16+ SCC	p16+ SCC	p16+ SCC
	Occult primary tissue imaged in area of FLIm Scan Region?[a]	Yes *R*-PT	Yes *L*-BOT	Yes *R*-BOT	No	No	No
	Occult primary tissue ultimately found in oropharynx?[a]	Yes *R*-PT	Yes *L*-BOT	Yes *R*-BOT	No	No	Yes Superior *R*-PT
	Other benign excised tissues[a]	*L*-PT *R*-BOT *R*-GTS	*R*-BOT *L*-BOT	*L*-PT	*L*-PT *L*-BOT *L*-GTS	*R*-BOT *R*-GTS	*L*-PT *R*-BOT *R*-GTS

Abbreviations: BOT, base of tongue; DPD, drinks per day; GTS, glossotonsillar sulcus; MA, methamphetamine; PPD, cigarette packs per day; PT, palatine tonsil; SCC, squamous cell carcinoma; p16+ SCC, HPV positive and HPV-mediated squamous cell carcinoma.
[a]"R" and "L" designate "Right" or "Left," respectively, with anatomy (e.g., R-PT refers to Right Palatine Tonsil).

TABLE 2 FLIm performance: ROC-AUC, sensitivity, and specificity

		ROC-AUC	Sensitivity	Specificity
p16+ SCC within FLIm scan area	Patient 1	0.97	92%	87%
	Patient 2	0.90	96%	81%
	Patient 3	0.82	99%	68%
No carcinoma within FLIm scan area	Patient 4			100%
	Patient 5			98%
	Patient 6			99%
	Mean	0.90 ± 0.06	96% ± 3.5%	89% ± 12.7%

Abbreviation: p16+ SCC, HPV-positive squamous cell carcinoma.

two key areas: (1) differentiation between oropharyngeal tissues that are benign versus those involved with p16+ SCC, and (2) demarcation of the extent of cancer.

The ability to correctly identify benign tissues uninvolved with HNSCCUP was demonstrated for the 3-patient cohort that comprised only benign tissues within the imaged FLIm scan region. Among these patients, the FLIm classifier yielded exceptionally high specificities, averaging 99% ± 1%, and correctly delineated the entire scanned regions of these tissues as benign. Ultimately, these patients each had multiple benign tissues of their oropharynx excised, which included palatine tonsils, base of tongue tissues, and glossotonsillar sulcus regions (Table 1). Due to the increased intraoperative procedure times, costs, pain, and functional implications from resection of patient's healthy tissue, there is strong motivation to prevent the unnecessary excision of benign tissues.

FLIm's ability to identify oropharyngeal tissues harboring HNSCCUP, as well as demarcate associated cancer margins, was demonstrated for the 3-patient cohort presenting with p16+ HNSCCUP tissue within the FLIm scan region. For these patients, HNSCCUP was successfully detected using the FLIm classifier. The best results were observed for Patient 1, where healthy tissue and

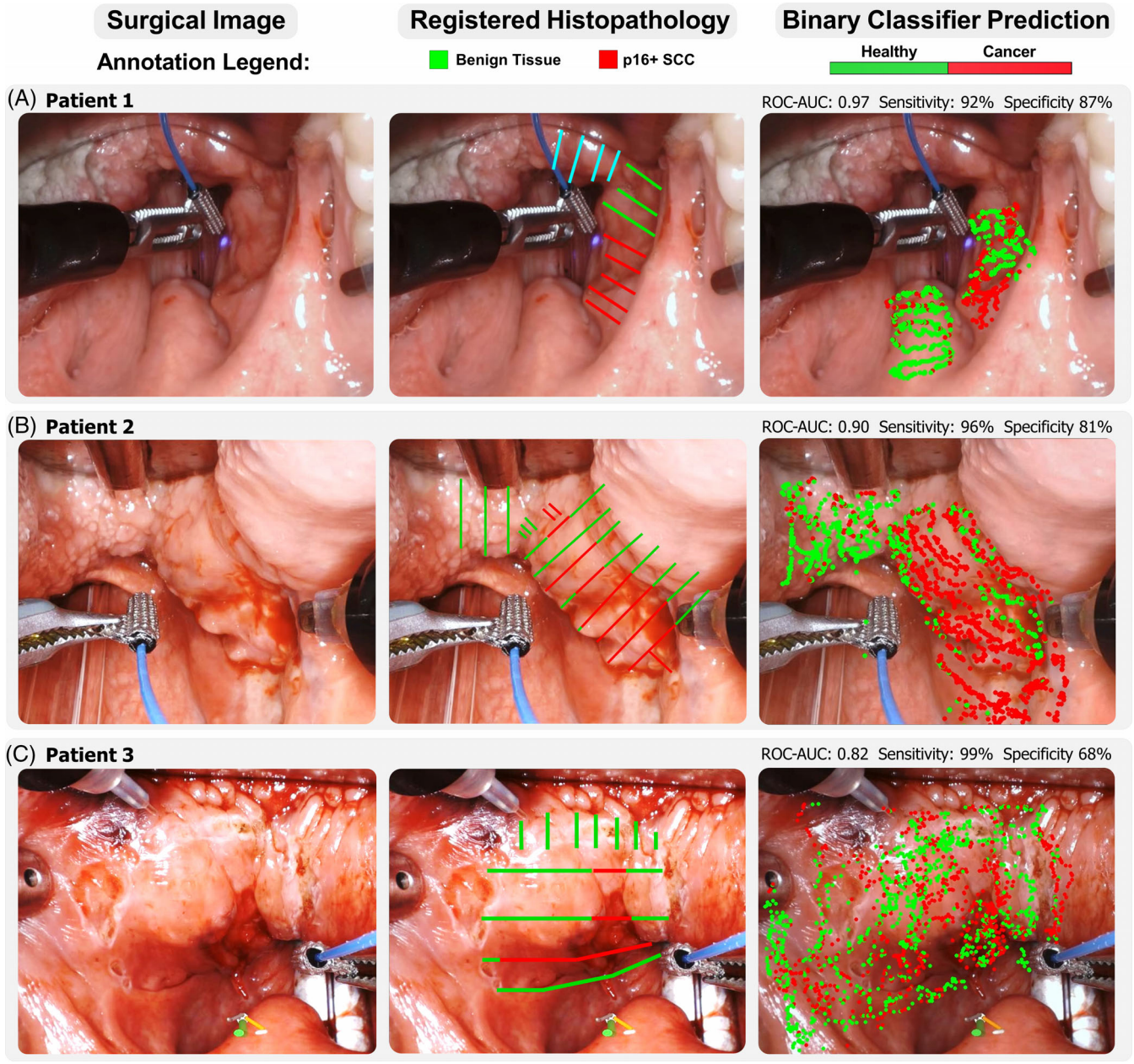

FIGURE 2 Patients with p16+ SCC within the imaged FLIm area. Each patient case study displays three tiles: (1) the original photograph of the surgical white light image, (2) the histopathology of the excised specimen registered in vivo, and (3) an overlay of the binary probability of cancer for each acquired spectral point-measurement. (A) Patient 1 with p16+ SCC of the right palatine tonsil. (B) Patient 2 with p16+ SCC of the left base of tongue. (C) Patient 3 with p16+ SCC of right base of tongue. [Color figure can be viewed at wileyonlinelibrary.com]

cancer were comprehensively differentiated. For Patient 2, the classifier performed well overall and fully demarcated the extent of the tumor. Cancer was successfully detected for Patient 3 presenting with p16+ HNSCCUP of the right base of tongue, however there was a low specificity (68%). Close inspection of Figure 2C reveals that the borders of the specimen were premarked with the da Vinci SP monopolar electrocautery tool prior to FLIm scanning, which is typically performed after the FLIm scan. In our previous work, we found that our FLIm signal is disrupted and altered by electrocautery, where effects on the FLIm signal extend many millimeters beyond the electrocautery site.[38] Figure 2C illustrates that many of the false positives occur around the cautery outline, thus offering a potential explanation for the low specificity. We hypothesize that FLIm could potentially differentiate between cancer and healthy tissue with accuracy on electrocauterized surfaces, however this has yet to be tested, and electrocauterized data was not included in the classifier training model.

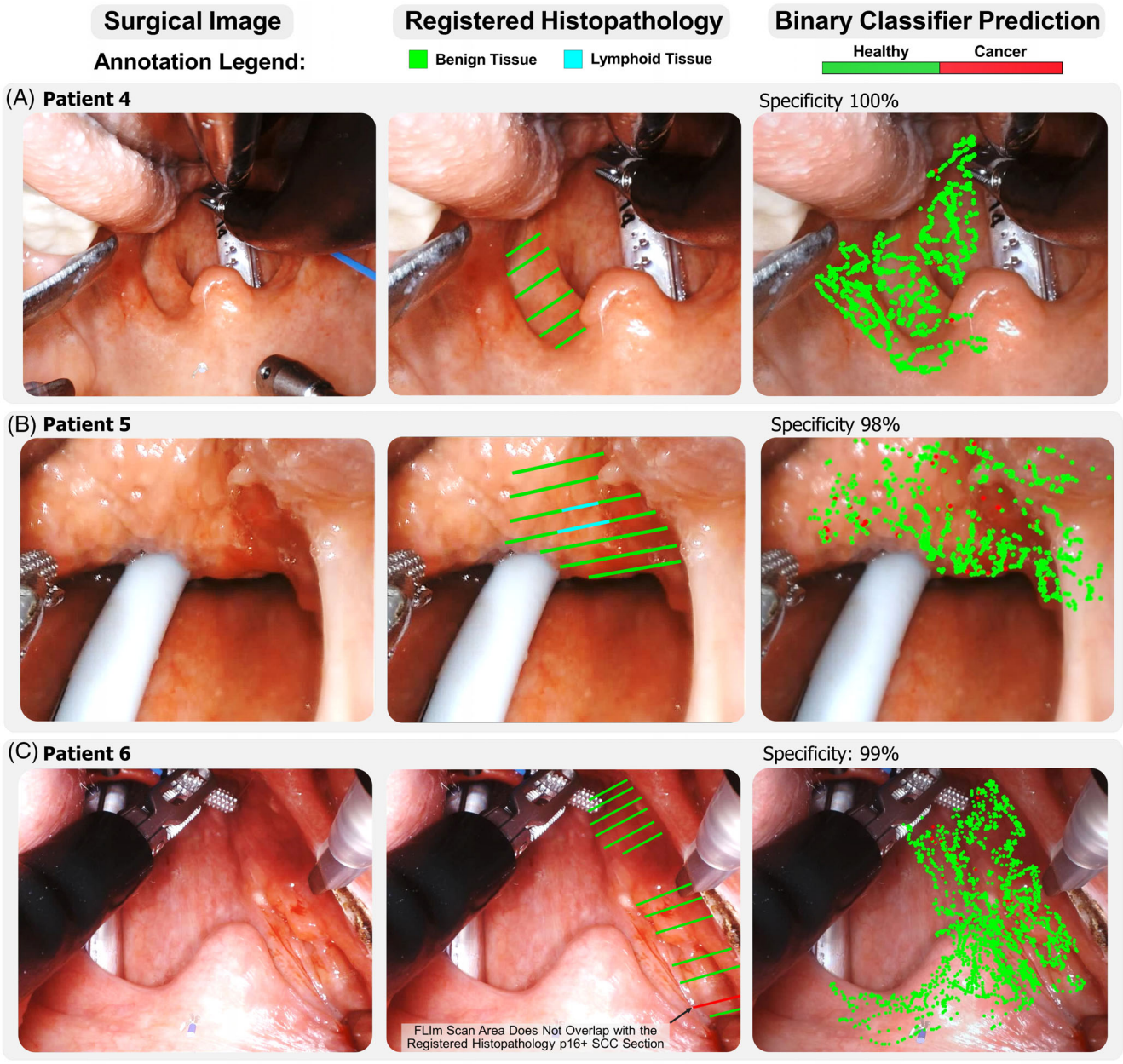

FIGURE 3 Patients with benign tissue only within the imaged FLIm area. Each patient case study displays three tiles: (1) the original photograph of the surgical white light image, (2) the histopathology of the excised specimen registered in vivo, and (3) an overlay of the binary probability of cancer for each acquired spectral point-measurement. (A) FLIm scan for Patient 4 of a benign left palatine tonsil. (B) FLIm scan for Patient 5 of a benign right base of tongue tissue. (C) Patient 6 case study illustrative of a challenging scenario where the FLIm scan area does not overlap with the area of cancer. For this patient with cancer of the right palatine tonsil, all benign tissue areas are correctly marked as healthy with 99% sensitivity, however the FLIm scan was not performed on the small area of the palatine tonsil where the occult primary p16+ SCC occurred. This case is illustrative of the importance of fully scanning an entire surgical region of interest with the FLIm technique to avoid missing a potential occult primary area. [Color figure can be viewed at wileyonlinelibrary.com]

4.1 | Exclusion criteria remarks

One HNSCCUP patient was not analyzed due to their medical history which designated this patient in the study's exclusion criteria. This patient routinely orally self-administered MA, which like crack-cocaine, is associated with severe oral health complications.[32] In brief, MA itself is acidic and when smoked or inhaled, has been linked to direct corrosive effects on oral tissues.[39,40] It has been found that MA is linked to increased expression of proinflammatory factors,[41] cellular senescence,[41] reduced oral tissue wound healing,[42] and

reduced saliva pH and buffering capacity.[43] Additionally, in murine models, MA has been found to facilitate host-mediated collagen degradation by increased expression and production of matrix metalloproteinases (MMPs).[42] Collectively, the effects of MA on oral cavity tissues demonstrates conserved properties to many cancer hallmarks,[30] therefore motivating this patient's exclusion from analysis due to confounding effects on the data. It is conceivable that with a large enough training dataset of MA patients, FLIm can differentiate benign MA-affected tissue from cancer, however this has yet to be tested.

Unlike the effect of MA, patient tobacco and ethanol (EtOH) use has not demonstrated apparent challenges in distinguishing benign tissue from cancer in our prior work.[19,20] One potential explanation for the classifier's resilience to this medical history may stem from the magnitude of patient data available (i.e., varied patient tobacco and EtOH use habits) to train the classifier's algorithm in predicting cancer probability.

4.2 | Study limitations and collective dataset remarks

Although the results obtained from this study are promising, the $N = 6$ HNSCCUP patient sample size is a key limitation; however, it should be emphasized that the rare nature of HNSCCUP makes the potential for patient recruitment in this single institution study limited. Like most high-volume head and neck cancer centers, we were stringent in our definition of HNSCCUP and only assigned patients to this designation after comprehensive preoperative workup were performed, including visual and endoscopic inspection, palpation, and comprehensive imaging. While validation was performed on six HNSCCUP patients, it is emphasized that training data in the classifier was developed using the larger 55-patient conventional SCC dataset, enabling the extrapolation of classification results on pilot study cohorts reliable. Along these lines, future investigation for the diagnostic utility of FLIm as a diagnostic adjunct for HNSCC should place emphasis on multi-institutional studies to obtain larger sample sizes.

A limitation of FLIm is demonstrated in Patient 6, where cancer only presented in a subtle area of the superior right palatine tonsil and resided outside of the FLIm scan. This case study is illustrative of the importance of thoroughly scanning the entire region of interest to assess the presence of tumor.

TORS has been incorporated as a successful strategy to detect unknown primary carcinoma of the oropharynx.[4,14–16] Several authors have demonstrated detection rates averaging as high as 80%.[44–46] While our study had a pathologic detection rate lower than those studies (50%), our practice is to aggressively look for the primary site with physical examination, imaging, and only consider the diagnosis of unknown primary if there is no suspicion of location based on preoperative and intraoperative findings. This difference in approach, and the size of our data sample, might explain the detection success discrepancy between our institution and the literature.

Collectively, these results, although preliminary, are promising for the potential identification of cancer of the unknown primary. These findings demonstrate potential to enhance surgical decision-making by aiding a surgeon in identifying candidate tissues of the oropharynx involved with carcinoma and in establishing the extent of cancer. If this potential to detect subtle mucosal-presenting carcinomas is confirmed in larger studies, FLIm could have dramatic impacts on radiation field reduction, or even the elimination of radiation therapy, in patients adequately treated with surgery alone. Along these lines, potential for FLIm to potentially guide initial biopsies and margins, which can reduce morbidity of unnecessary tonsillectomies/biopsies on oropharyngeal tissues that do not harbor malignancy.

5 | CONCLUSIONS

FLIm, in combination with the conventional diagnostic workup for HNSCCUP, may be a useful adjunctive modality for detecting primary tumors. This preliminary investigation demonstrated that FLIm, integrated with TORS, may aid a surgeon in rapidly and non-invasively screening patients for mucosa-presenting (<250 μm from tissue surface) p16+ HNSCCUP. The results suggest that FLIm can correctly demarcate entire benign tissues of the oropharynx and thus indicate to a surgeon that tissues suspected of occult primary are uninvolved with carcinoma. For all patients presenting with p16+ HNSCCUP in the FLIm scan region, the method correctly identified the presence and location of the occult primary with overall strong performance, in addition to accurately identifying uninvolved healthy functional tissue. Ultimately, these results demonstrate potential to reduce surgical procedure times, preserve functional healthy tissue, and enable enhanced intraoperative decision-making for the benefit of the patient.

ACKNOWLEDGMENTS

This project was supported by the National Institutes of Health (Grant: R01 CA187427). This is an academic-industry partnership grant between UC Davis and Intuitive Surgical, Inc. We acknowledge Dr. Jonathan Sorger

of Intuitive Surgical for his mentorship. The authors thank our clinical coordinators Angela Beliveau, M.P.H., CCRP (Senior Clinical Research Coordinator) and Randev Sandhu, CCRP (Clinical Research Supervisor) at the University of California, Davis Medical Center Department of Otolaryngology for their many contributions to enroll and consent patients in our study, maintain patient files and medical history documents, and disseminate research study information to our team. We would like to also thank Xiangnan Zhou for improving the stability of the FLIm system software and Takanori Fukazawa for identifying motion correction methods to improve data registration as demonstrated in our prior study.[18]

CONFLICT OF INTEREST

The author declares that there is no conflict of interest that could be perceived as prejudicing the impartiality of the research reported.

AUTHOR CONTRIBUTIONS

Brent W. Weyers collected and analyzed all patient data in the study, prepared all written content in the manuscript, designed all tables, and created the figures. Andrew C. Birkeland provided the primary intellectual contribution related to this manuscript concept. Mark A. Marsden led the machine learning classification endeavor and performed all computations output from the classifier. Athena Tam, Julien Bec, and Roberto P. Frusciante assisted with the acquisition, preparation, and interpretation of data, in addition to edits and review of content featured in this manuscript. Dorina Gui reviewed the manuscript and served as the primary pathologist on record for the study. Andrew C. Birkeland, Arnaud F. Bewley, Marianne Abouyared, and Donald Gregory Farwell each participated in acquiring data for our research study, provided intellectual contributions, and assisted in the editing and review of this manuscript. Laura Marcu, Donald Gregory Farwell, and Julien Bec jointly supervised the entire research effort and provided support for the analysis and interpretation of the data.

DATA AVAILABILITY STATEMENT

The data supporting the findings of this study are available from the corresponding author, and will be furnished upon reasonable request.

ORCID

Brent W. Weyers https://orcid.org/0000-0002-1939-3401
Andrew C. Birkeland https://orcid.org/0000-0003-2500-2857
Mark A. Marsden https://orcid.org/0000-0002-8480-9653
Athena Tam https://orcid.org/0000-0001-6166-2487
Julien Bec https://orcid.org/0000-0003-1222-4071
Roberto P. Frusciante https://orcid.org/0000-0001-9305-9922
Dorina Gui https://orcid.org/0000-0002-1500-6689
Arnaud F. Bewley https://orcid.org/0000-0002-1524-1806
Marianne Abouyared https://orcid.org/0000-0002-2779-5494
Laura Marcu https://orcid.org/0000-0003-2369-0748
Donald Gregory Farwell https://orcid.org/0000-0003-3421-4202

REFERENCES

1. Mackenzie K, Watson M, Jankowska P, Bhide S, Simo R. Investigation and management of the unknown primary with metastatic neck disease: United Kingdom National Multidisciplinary Guidelines. *J Laryngol Otol*. 2016;130(S2):S170-S175. doi:10.1017/s0022215116000591
2. Pavlidis N, Khaled H, Gaafar R. A mini review on cancer of unknown primary site: a clinical puzzle for the oncologists. *J Adv Res*. 2015;6:375-382. doi:10.1016/j.jare.2014.11.007
3. Pavlidis N, Pentheroudakis G. Cancer of unknown primary site. *Lancet*. 2012;379:1428-1435. doi:10.1016/S0140-6736(11)61178-1
4. Motz K, Qualliotine JR, Rettig E, Richmon JD, Eisele DW, Fakhry C. Changes in unknown primary squamous cell carcinoma of the head and neck at initial presentation in the era of human papillomavirus. *JAMA Otolaryngol Head Neck Surg*. 2016;142(3):223-228. doi:10.1001/jamaoto.2015.3228
5. Ofo E, Spiers H, Kim D, Duvvuri U. Transoral robotic surgery and the unknown primary. *ORL J Otorhinolaryngol Relat Spec*. 2018;80(3–4):148-155. doi:10.1159/000490596
6. Strojan P, Ferlito A, Medina JE, et al. Contemporary management of lymph node metastases from an unknown primary to the neck: I. a review of diagnostic approaches. *Head Neck*. 2013;35(1):123-132. doi:10.1002/hed.21898
7. Rassy E, Nicolai P, Pavlidis N. Comprehensive management of HPV-related squamous cell carcinoma of the head and neck of unknown primary. *Head Neck*. 2019;41(10):3700-3711. doi:10.1002/hed.25858
8. Zengel P, Assmann G, Mollenhauer M, et al. Cancer of unknown primary originating from oropharyngeal carcinomas are strongly correlated to HPV positivity. *Virchows Arch*. 2012;461(3):283-290. doi:10.1007/s00428-012-1290-3
9. O'Rorke MA, Ellison MV, Murray LJ, Moran M, James J, Anderson LA. Human papillomavirus related head and neck cancer survival: a systematic review and meta-analysis. *Oral Oncol*. 2012;48(12):1191-1201. doi:10.1016/j.oraloncology.2012.06.019
10. Lewis JS, Shelton J, Kuhs KL, Smith DK. p16 immunohistochemistry in oropharyngeal squamous cell carcinoma using the E6H4 antibody clone: a technical method study for optimal dilution. *Head Neck Pathol*. 2018;12(4):440-447. doi:10.1007/s12105-017-0871-5
11. Dhere VR, Escott CE, Tian S, et al. The omission of intentional primary site radiation following transoral robotic surgery in

59 patients: no local-regional failures. *Head Neck*. 2022;44(2):382-390. doi:10.1002/HED.26928
12. Fu TS, Foreman A, Goldstein DP, De Almeida JR. The role of transoral robotic surgery, transoral laser microsurgery, and lingual tonsillectomy in the identification of head and neck squamous cell carcinoma of unknown primary origin: a systematic review. *J Otolaryngol Head Neck Surg*. 2016;45(1):28. doi:10.1186/s40463-016-0142-6
13. Parhar HS, Shimunov D, Brody RM, et al. Revisiting the recommendation for contralateral tonsillectomy in HPV-associated tonsillar carcinoma. *Otolaryngol Head Neck Surg (United States)*. 2021;164(6):1222-1229. doi:10.1177/0194599820968800
14. Channir HI, Rubek N, Nielsen HU, et al. Transoral robotic surgery for the management of head and neck squamous cell carcinoma of unknown primary. *Acta Otolaryngol*. 2015;135(10):1051-1057. doi:10.3109/00016489.2015.1052983
15. Patel SA, Magnuson JS, Holsinger FC, et al. Robotic surgery for primary head and neck squamous cell carcinoma of unknown site. *JAMA Otolaryngol Head Neck Surg*. 2013;139(11):1203-1211. doi:10.1001/jamaoto.2013.5189
16. Fu TS, Foreman A, Goldstein DP, De Almeida JR. The role of transoral robotic surgery, transoral laser microsurgery, and lingual tonsillectomy in the identification of head and neck squamous cell carcinoma of unknown primary origin: a systematic review. *J Otolaryngol Head Neck Surg*. 2016;45(1):1-10. doi:10.1186/s40463-016-0142-6
17. Gorpas D, Phipps J, Bec J, et al. Autofluorescence lifetime augmented reality as a means for real-time robotic surgery guidance in human patients. *Sci Rep*. 2019;9(1):1187. doi:10.1038/s41598-018-37237-8
18. Marsden M, Fukazawa T, Deng Y-C, et al. FLImBrush: dynamic visualization of intraoperative free-hand fiber-based fluorescence lifetime imaging. *Biomed Opt Express*. 2020;11(9):5166-5180. doi:10.1364/boe.398357
19. Weyers BW, Marsden M, Sun T, et al. Fluorescence lifetime imaging for intraoperative cancer delineation in transoral robotic surgery. *Transl Biophotonics*. 2019;1:e201900017. doi:10.1002/tbio.201900017
20. Marsden M, Weyers BW, Bec J, et al. Intraoperative margin assessment in oral and oropharyngeal cancer using label-free fluorescence lifetime imaging and machine learning. *IEEE Trans Biomed Eng*. 2021;68(3):857-868. doi:10.1109/TBME.2020.3010480
21. Bec J, Vela D, Phipps JE, et al. Label-free visualization and quantification of biochemical markers of atherosclerotic plaque progression using intravascular fluorescence lifetime. *JACC Cardiovasc Imaging*. 2020;18:1832-1842. doi:10.1016/j.jcmg.2020.10.004
22. Bec J, Shaik TA, Krafft C, et al. Investigating origins of FLIm contrast in atherosclerotic lesions using combined FLIm-Raman spectroscopy. *Front Cardiovasc Med*. 2020;7:122. doi:10.3389/fcvm.2020.00122
23. Bec J, Phipps JE, Gorpas D, et al. In vivo label-free structural and biochemical imaging of coronary arteries using an integrated ultrasound and multispectral fluorescence lifetime catheter system. *Sci Rep*. 2017;7(1):8960. doi:10.1038/s41598-017-08056-0
24. Unger J, Hebisch C, Phipps JE, et al. Real-time diagnosis and visualization of tumor margins in excised breast specimens using fluorescence lifetime imaging and machine learning. *Biomed Opt Express*. 2020;11(3):1216-1230. doi:10.1364/boe.381358
25. Alfonso-Garcia A, Bec J, Sridharan Weaver S, et al. Real-time augmented reality for delineation of surgical margins during neurosurgery using autofluorescence lifetime contrast. *J Biophotonics*. 2019;9:e201900108. doi:10.1002/jbio.201900108
26. Sridharan S, Huang EC, Campbell MJ, Marcu L. Fluorescence lifetime imaging for intra-operative guidance during thyroid surgery. *Opt Life Sci Congr*. 2017;Part F63-OMP 2017:OmM3D.2. doi:10.1364/OMP.2017.OMM3D.2
27. Alfonso-Garcia A, Bec J, Weyers B, et al. Mesoscopic fluorescence lifetime imaging: fundamental principles, clinical applications, and future directions. *J Biophotonics*. Published online March 12, 2021: 14 e202000472. 10.1002/jbio.202000472
28. Marcu L, French PMW, Elson DS. *Fluorescence Lifetime Spectroscopy and Imaging: Principles and Applications in Biomedical Diagnostics*. CRC Press; 2014.
29. Lakowicz JR, Szmacinski H, Nowaczyk K, Johnson ML. Fluorescence lifetime imaging of free and protein-bound NADH. *Proc Natl Acad Sci U S A*. 1992;89(4):1271-1275. doi:10.1073/pnas.89.4.1271
30. Hanahan D, Weinberg RA. Hallmarks of cancer: the next generation. *Cell*. 2011;144(5):646-674. doi:10.1016/j.cell.2011.02.013
31. Al-Mulki K, Hamilton J, Kaka AS, et al. Narrowband imaging for p16+ unknown primary squamous cell carcinoma prior to transoral robotic surgery. *Otolaryngol Head Neck Surg (United States)*. 2020;163(6):1198-1201. doi:10.1177/0194599820933204
32. Shekarchizadeh H, Khami MR, Mohebbi SZ, Ekhtiari H, Virtanen JI. Oral health of drug abusers: a review of health effects and care. *Iran J Public Health*. 2013;42(9):929-940.
33. Liu J, Sun Y, Qi J, Marcu L. A novel method for fast and robust estimation of fluorescence decay dynamics using constrained least-squares deconvolution with Laguerre expansion. *Phys Med Biol*. 2012;57(4):843-865. doi:10.1088/0031-9155/57/4/843
34. Gorpas D, Ma D, Bec J, Yankelevich DR, Marcu L. Real-time visualization of tissue surface biochemical features derived from fluorescence lifetime measurements. *IEEE Trans Med Imaging*. 2016;35(8):1802-1811. doi:10.1109/TMI.2016.2530621
35. Yankelevich DR, Ma D, Liu J, et al. Design and evaluation of a device for fast multispectral time-resolved fluorescence spectroscopy and imaging. *Rev Sci Instrum*. 2014;85(3):34303. doi:10.1063/1.4869037
36. Aran D, Camarda R, Odegaard J, et al. Comprehensive analysis of normal adjacent to tumor transcriptomes. *Nat Commun*. 2017;8(1):1-14. doi:10.1038/s41467-017-01027-z
37. Breiman L. Random forests. *Mach Learn*. 2001;45(1):5-32. doi:10.1023/A:1010933404324
38. Lagarto JL, Phipps JE, Faller L, et al. Electrocautery effects on fluorescence lifetime measurements: an in vivo study in the oral cavity. *J Photochem Photobiol B Biol*. 2018;185:90-99. doi:10.1016/j.jphotobiol.2018.05.025
39. Teoh L, Moses G, McCullough M. Oral manifestations of illicit drug use. *Aust Dent J*. 2019;64(3):213-222. doi:10.1111/adj.12709
40. De-Carolis C, Boyd GA, Mancinelli L, Pagano S, Eramo S. Methamphetamine abuse and "meth mouth" in Europe. *Med Oral Patol Oral Cir Bucal*. 2015;20(2):e205-e210. doi:10.4317/medoral.20204

41. Astarita G, Avanesian A, Grimaldi B, et al. Methamphetamine accelerates cellular senescence through stimulation of de novo ceramide biosynthesis. *Published Online*. 2015;10:e0116961. doi:10.1371/journal.pone.0116961
42. Mihu MR, Roman-Sosa J, Varshney AK, et al. Methamphetamine alters the antimicrobial efficacy of phagocytic cells during methicillin-resistant staphylococcus aureus skin infection. *MBio*. 2015;6(6):e01622-15. doi:10.1128/mBio.01622-15
43. Hamamoto DT, Rhodus NL. Methamphetamine abuse and dentistry. *Oral Dis*. 2009;15(1):27-37. doi:10.1111/j.1601-0825.2008.01459.x
44. Hatten KM, O'Malley BW, Bur AM, et al. Transoral robotic surgery-assisted endoscopy with primary site detection and treatment in occult mucosal primaries. *JAMA Otolaryngol Head Neck Surg*. 2017;143(3):267-273. doi:10.1001/jamaoto.2016.3419
45. Weert S, Rijken JA, Plantone F, et al. A systematic review on Transoral robotic surgery (TORS) for carcinoma of unknown primary origin: Has tongue base mucosectomy become indispensable? *Clin Otolaryngol*. 2020;45(5):732-738. doi:10.1111/coa.13565
46. Geltzeiler M, Doerfler S, Turner M, et al. Transoral robotic surgery for management of cervical unknown primary squamous cell carcinoma: updates on efficacy, surgical technique and margin status. *Oral Oncol*. 2017;66:9-13. doi:10.1016/j.oraloncology.2016.12.033

SUPPORTING INFORMATION

Additional supporting information may be found in the online version of the article at the publisher's website.

How to cite this article: Weyers BW, Birkeland AC, Marsden MA, et al. Intraoperative delineation of p16+ oropharyngeal carcinoma of unknown primary origin with fluorescence lifetime imaging: Preliminary report. *Head & Neck*. 2022;44(8):1765-1776. doi:10.1002/hed.27078